Supporting Information

Modulating Hydrocarbon Coverage on Mo-Doped RuO_2 Anodes Enables Energy-Efficient and Selective Kolbe Electrolysis

Jian Yang,[a] Fan Lin,[a] Shaojie Lei,[a] Zichen Li,[a] Hui Zhang,[a] Zhibao Huo[a] and Dezhang Ren*[a]

[a] *College of Oceanography and Ecological Science, Shanghai Ocean University, No.999, Hucheng Ring Road, Shanghai, 201306, China*

* Corresponding Author:

E-mail: dzren@shou.edu.cn

S1. Supporting Graphs

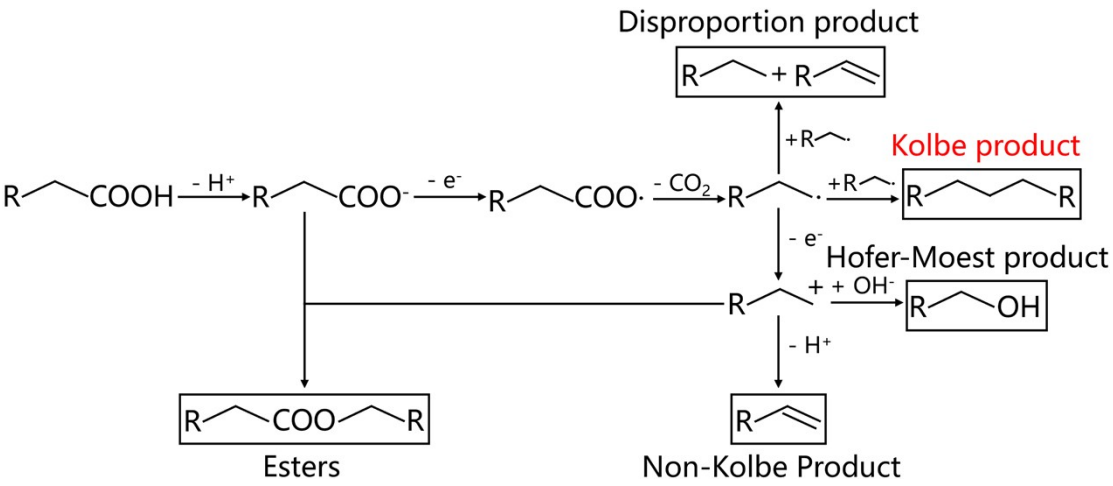

Fig. S1. Proposed reaction mechanism for the Kolbe electrolysis of carboxylic acids.

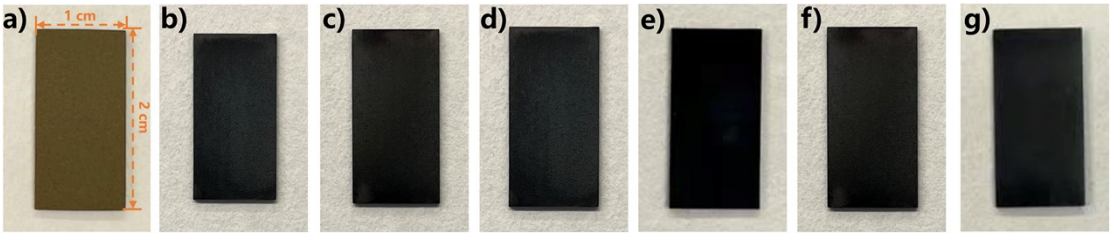

Fig. S2. Photographs of the Ti Substrate, the RuO_2 electrode, and the electrodes doped with different metals: (a) Ti Substrate after calcination at 470 °C, (b) RuO_2 electrode, (c) RuO_2-5%Mo electrode, (d) RuO_2-5%Ta electrode, (e) RuO_2-5%Zr electrode, (f) RuO_2-5%W electrode, (g) RuO_2-5%Sn electrode.

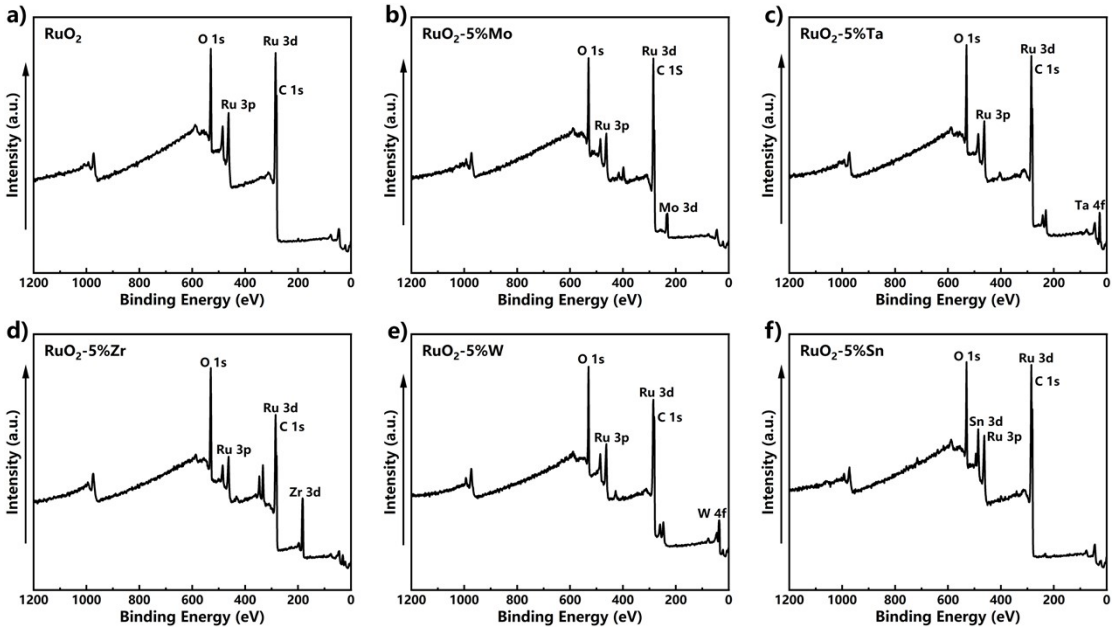

Fig. S3. XPS survey spectra of the RuO_2 electrode and electrodes doped with different metals: (a) RuO_2 electrode, (b) RuO_2-5%Mo electrode, (c) RuO_2-5%Ta electrode, (d) RuO_2-5%Zr electrode, (e) RuO_2-5%W electrode, (f) RuO_2-5%Sn electrode.

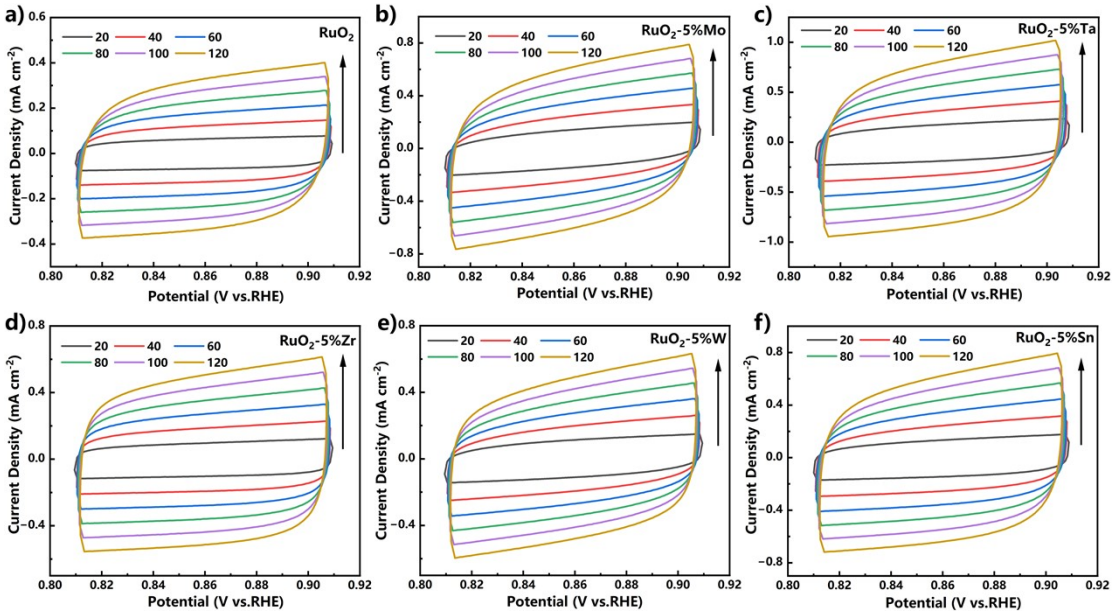

Fig. S4. CV curves of the RuO_2 and doped electrodes in 0.5 M KOH solution at different scan rates: (a) RuO_2, (b) RuO_2-5%Mo, (c) RuO_2-5%Ta, (d) RuO_2-5%Zr, (e) RuO_2-5%W, (f) RuO_2-5%Sn. All measurements were conducted using a three-electrode system with an Ag/AgCl reference electrode.

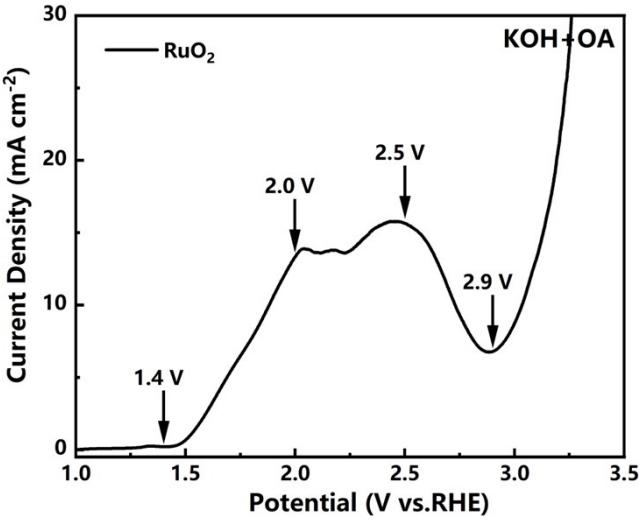

Fig. S5. LSV curve of the RuO_2 electrode in 0.5 M KOH + 0.5 M OA solution at a scan rate of 20 mV s^{-1}.

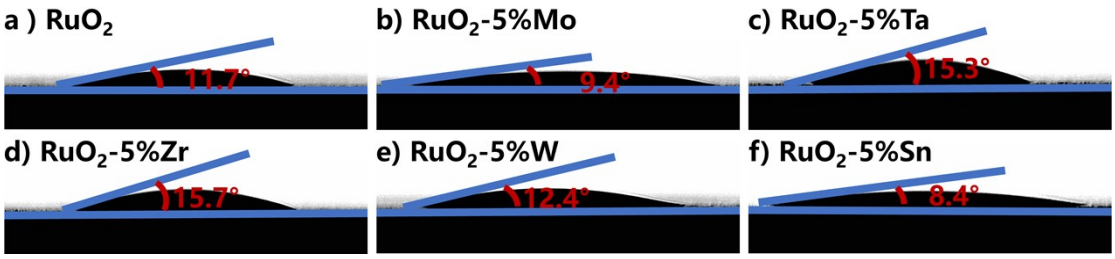

Fig. S6. Contact angle images of the fresh (as-prepared) RuO_2 and doped electrodes: (a) RuO_2, (b) RuO_2-5%Mo, (c) RuO_2-5%Ta, (d) RuO_2-5%Zr, (e) RuO_2-5%W, (f) RuO_2-5%Sn.

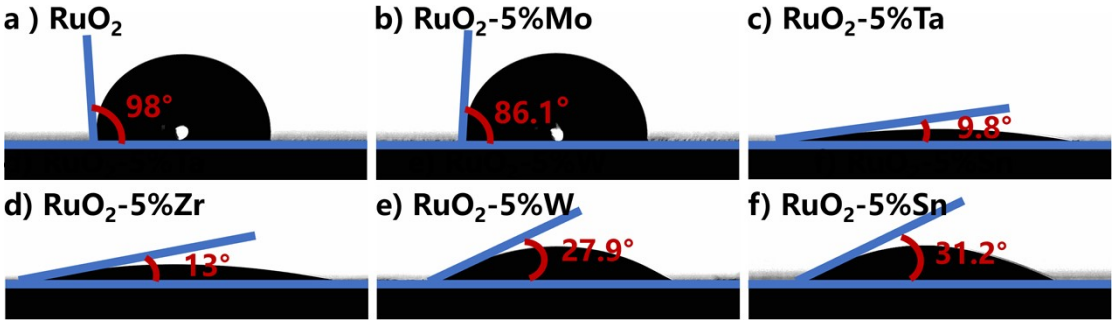

Fig. S7. Contact angle images of the RuO_2 and doped electrodes after the LSV measurement: (a) RuO_2, (b) RuO_2-5%Mo, (c) RuO_2-5%Ta, (d) RuO_2-5%Zr, (e) RuO_2-5%W, (f) RuO_2-5%Sn.

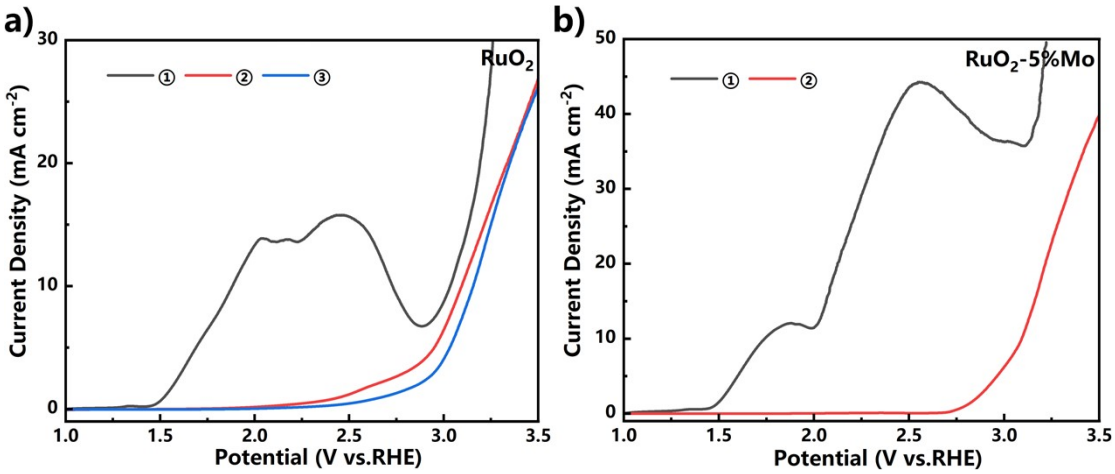

Fig. S8. Consecutive LSV scans of RuO_2 electrode and RuO_2-5%Mo electrode. (a) RuO_2 electrode, (b) RuO_2-5%Mo electrode. Electrolyte: 0.5 M KOH + 0.5 M OA. Scan rate: 20 mV s^{-1}. Note: The electrode surface was not rinsed between consecutive scans, which were performed directly in the same electrolyte.

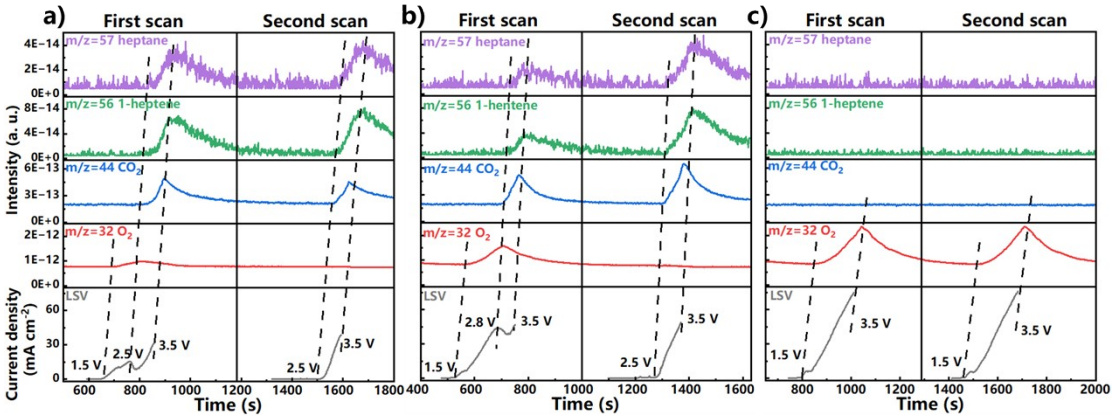

Fig. S9. DEMS results for the different electrodes: (a) RuO_2, (b) RuO_2-5%Mo, (c) RuO_2-5%Zr. The graphs display two consecutive LSV scans along with the corresponding signals of volatile products. Note: tetradecane (C_{14}), the dimer product of Kolbe electrolysis, is not detectable by DEMS due to its extremely low vapor pressure at room temperature. The lag of the MS signal is caused by the time required for the transfer of gases from the electrode surface to the mass spectrometer detector.

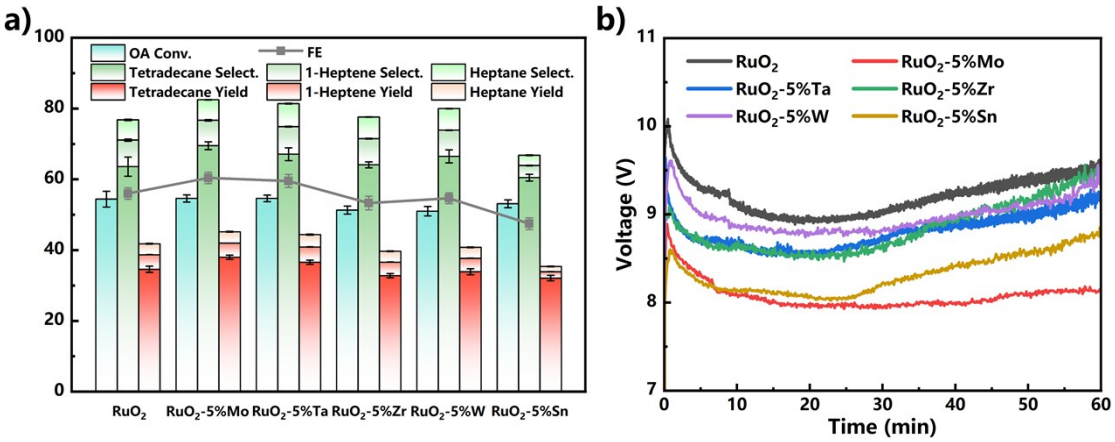

Fig. S10. Electrochemical performance of the RuO_2 and doped electrodes during galvanostatic electrolysis: (a) OA conversion, selectivity, yield of heptane, 1-heptene, tetradecane, and the overall Faradaic efficiency (FE), (b) cell voltage profile. The measurements were performed directly using a DC power supply in a two-electrode system; the voltages reported are the actual measured values.

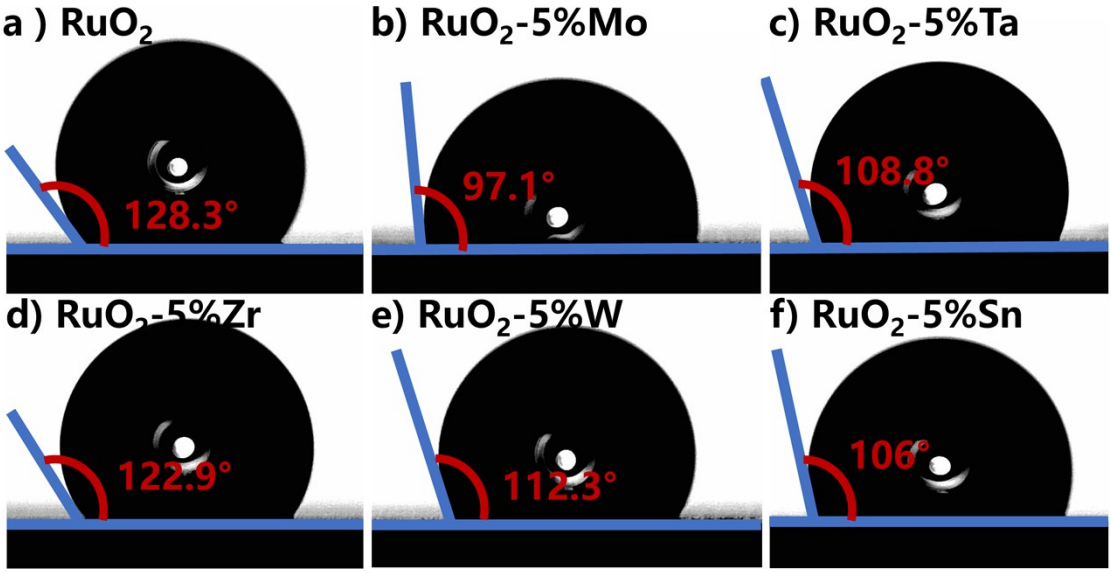

Fig. S11. Contact angle images of the RuO_2 and doped electrodes after galvanostatic electrolysis: (a) RuO_2, (b) RuO_2-5%Mo, (c) RuO_2-5%Ta, (d) RuO_2-5%Zr, (e) RuO_2-5%W, (f) RuO_2-5%Sn.

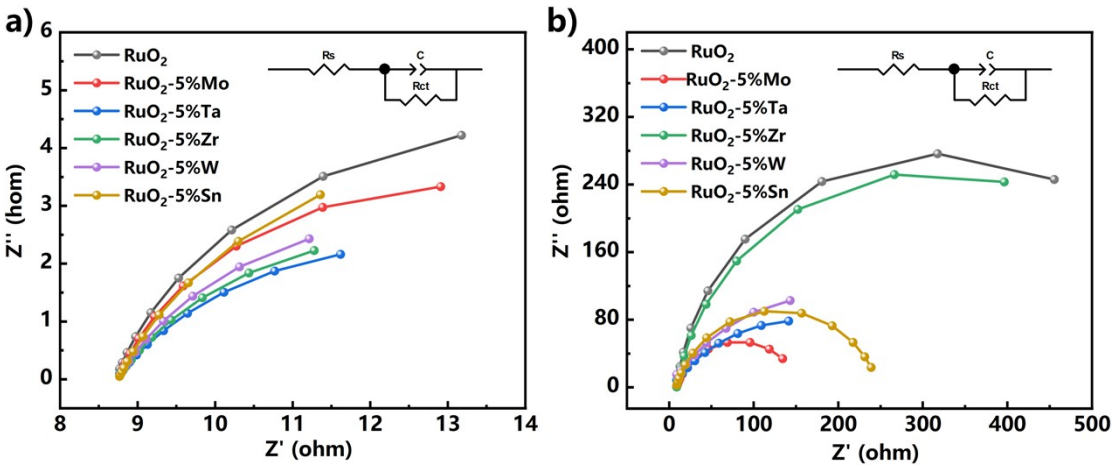

Fig. S12. Nyquist plots of the RuO_2 and metal-doped electrodes recorded after the passage of the same charge quantity, comparing the electrodes before and after 60 min of galvanostatic electrolysis. (a) before electrolysis, (b) after 60 min of galvanostatic electrolysis. Electrolyte: 0.5 M KOH + 0.5 M OA. The comparison illustrates the evolution of the surface coverage and its influence on the electrode's charge transfer resistance during extended operation.

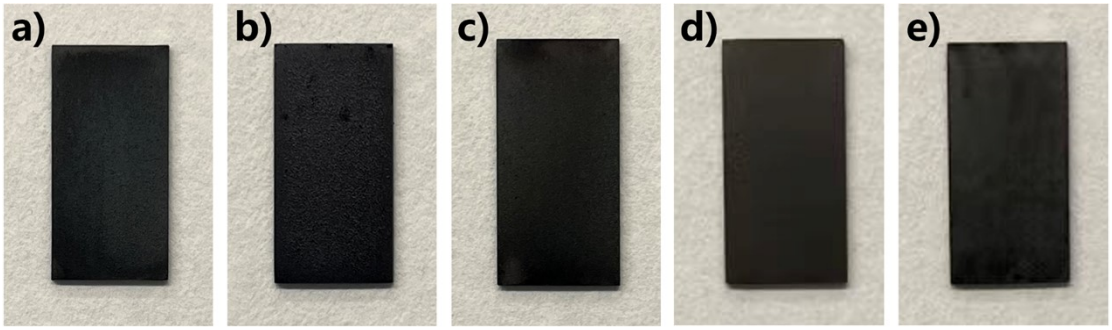

Fig. S13. Photographs of the RuO_2 electrodes with different Mo doping levels: (a) RuO_2, (b) RuO_2-1%Mo, (c) RuO_2-5%Mo, (d) RuO_2-10%Mo, (e) RuO_2-20%Mo.

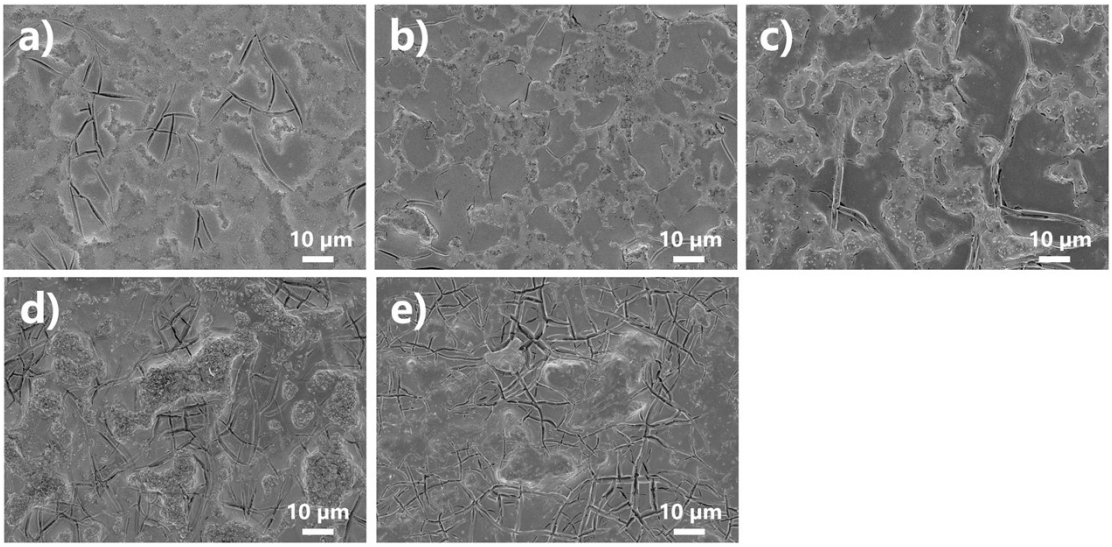

Fig. S14. Low-magnification SEM images of the RuO_2 electrodes with different Mo doping levels: (a) RuO_2, (b) RuO_2-1%Mo, (c) RuO_2-5%Mo, (d) RuO_2-10%Mo, (e) RuO_2-20%Mo. The scale bar is 10 μm.

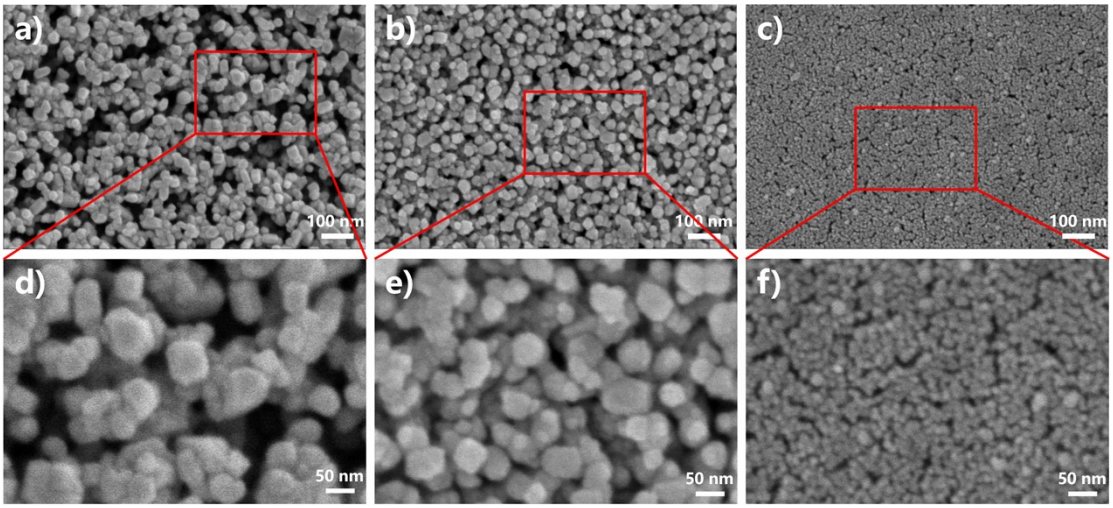

Fig. S15. High-magnification SEM images of the RuO_2 electrodes with different Mo doping levels: (a, d) RuO_2, (b, e) RuO_2-1%Mo, (c, f) RuO_2-20%Mo. The scale bars in panels (a-c) and (d-f) are 100 nm and 50 nm, respectively.

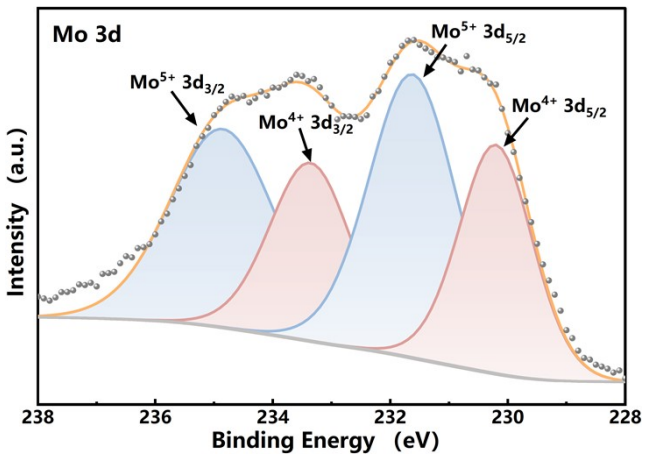

Fig. S16. High-resolution XPS spectrum of Mo 3d acquired from the RuO_2-5%Mo electrode, showing the chemical states of Mo.

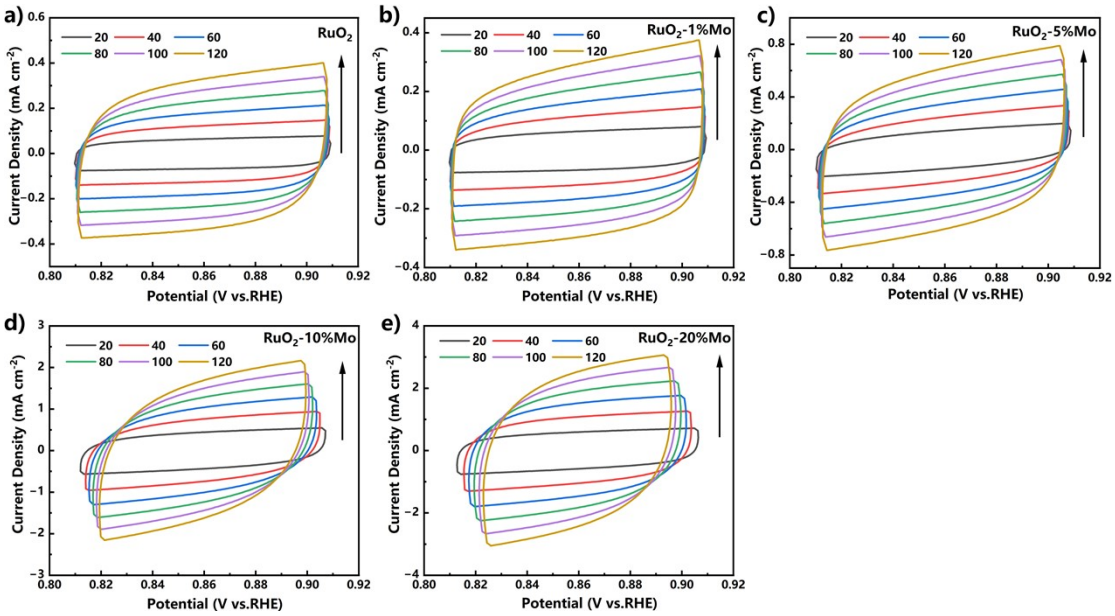

Fig. S17. CV curves of the RuO_2 electrodes with different Mo doping levels at various scan rates: (a) RuO_2, (b) RuO_2-1%Mo, (c) RuO_2-5%Mo, (d) RuO_2-10%Mo, (e) RuO_2-20%Mo. The measurement conditions are the same as those described for Fig. S4.

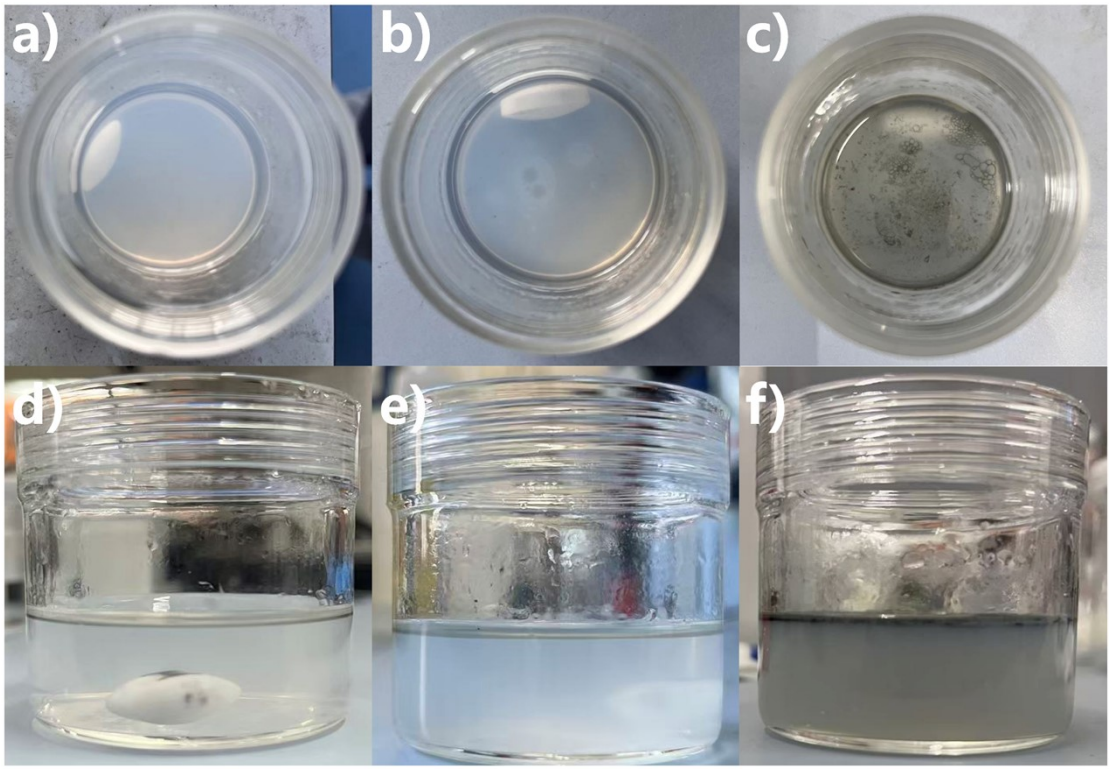

Fig. S18. Photographs of the electrolytes after galvanostatic electrolysis for the RuO_2 electrodes with different Mo doping levels: (a, d) RuO_2, (b, e) RuO_2-5%Mo, (c, f) RuO_2-10%Mo.

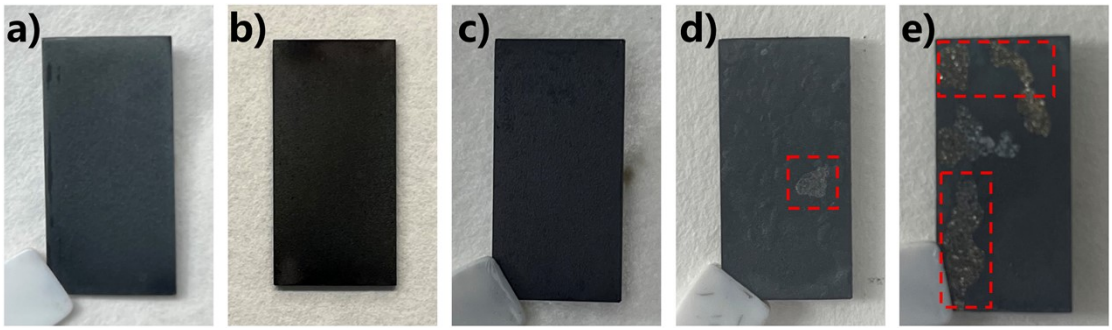

Fig. S19. Photographs of the RuO_2-5%Mo electrodes prepared at different calcination temperatures: (a) 300 °C, (b) 470 °C, (c) 600 °C, (d) 650 °C, (e) 700 °C.

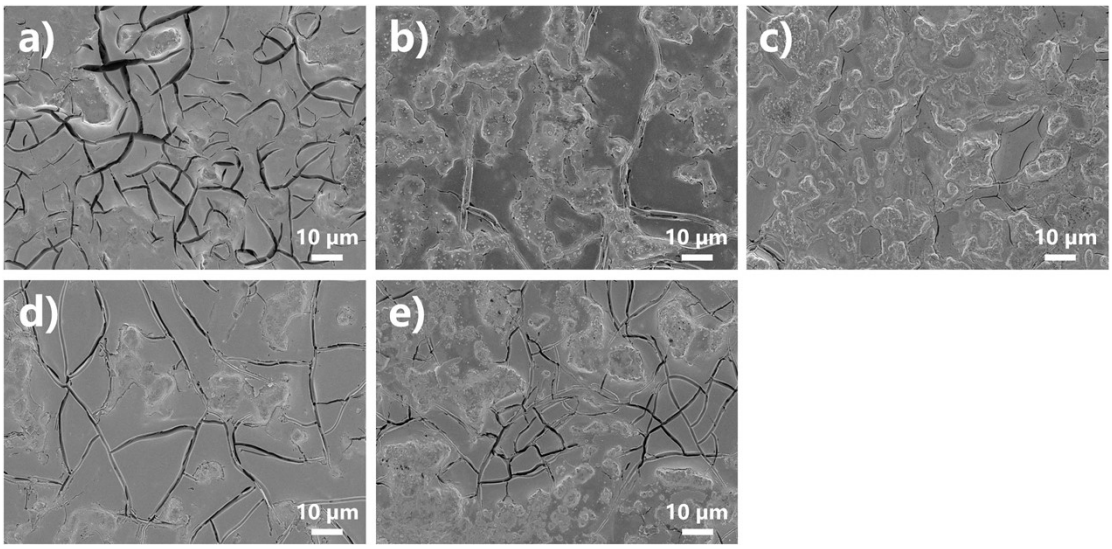

Fig. S20. Low-magnification SEM images of the RuO_2-5%Mo electrodes prepared at different calcination temperatures: (a) 300 °C, (b) 470 °C, (c) 600 °C, (d) 650 °C, (e) 700 °C. The scale bar is 10 μm.

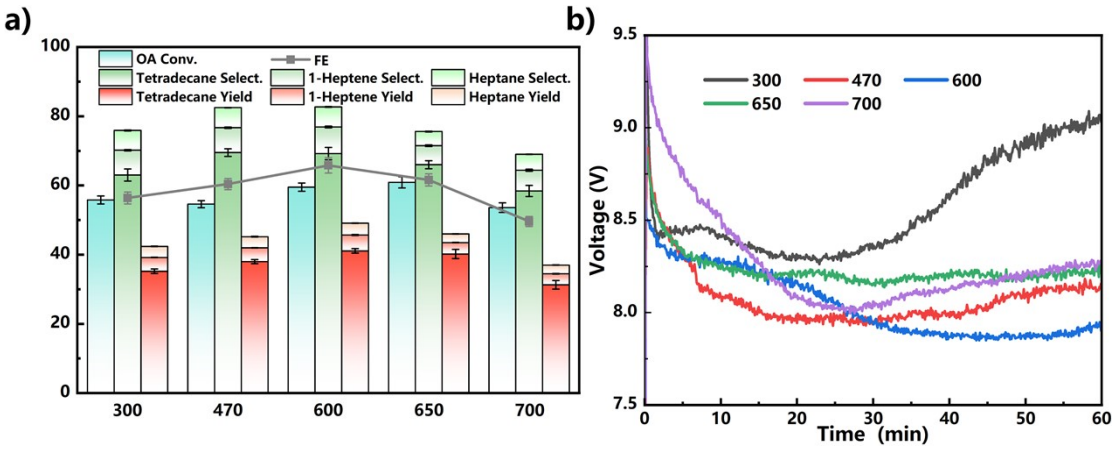

Fig. S21. Electrolysis performance of the RuO_2-5%Mo electrodes prepared at different calcination temperatures: (a) OA conversion, selectivity, yield of heptane, 1-heptene, tetradecane, and the overall Faradaic efficiency (FE). (b) Cell voltage profiles during galvanostatic electrolysis. Note: The measurements were performed directly using a DC power supply in a two-electrode system; the voltages reported are the actual measured values.

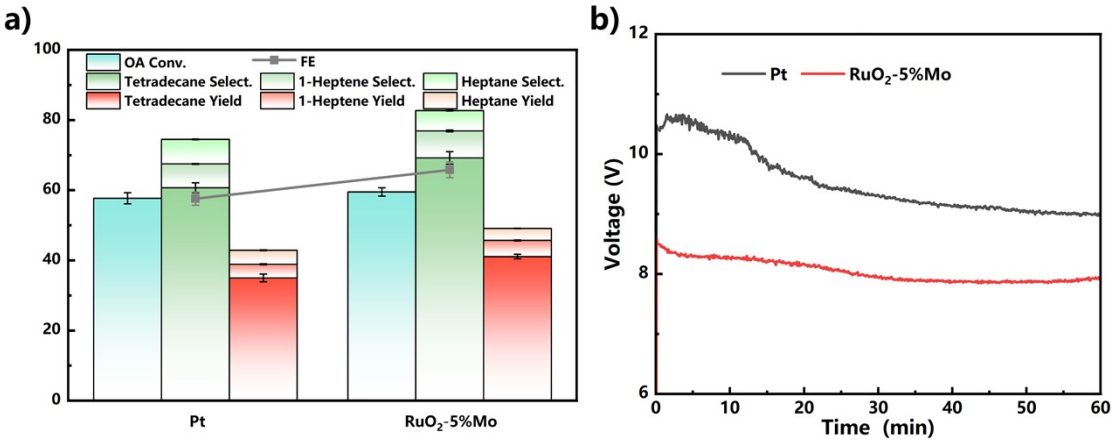

Fig. S22. Comparison of the electrolysis performance between the Pt electrode and the RuO_2-5%Mo electrode under identical reaction conditions: (a) OA conversion, selectivity, yield of heptane, 1-heptene, tetradecane, and the overall Faradaic efficiency (FE). (b) Cell voltage profiles during galvanostatic electrolysis. Note: The measurements were performed directly using a DC power supply in a two-electrode system; the voltages reported are the actual measured values.

S2. Supporting Tables

Table S1. Ionic radii and electronegativity of the different metallic elements.

Element	Ionic Radius (Å)	Electronegativity
Ru^{4+}	0.62	2.2
Mo^{6+}	0.59	2.16
Ta^{5+}	0.64	1.5
Zr^{4+}	0.72	1.33
W^{6+}	0.6	2.36
Sn^{4+}	0.69	1.96

Table S2. Mass and thickness changes of the Ti Substrate, RuO_2 electrode, and doped electrodes before and after calcination.

	Mass before Coating (g)	Mass after Coating (g)	Mass increase (g)
Ti Substrate	0.846	0.846	0
RuO_2	0.852	0.864	0.012±0.002
RuO_2-5%Mo	0.843	0.856	0.013±0.002
RuO_2-5%Ta	0.844	0.854	0.010±0.001
RuO_2-5%Zr	0.845	0.857	0.012±0.002
RuO_2-5%W	0.842	0.851	0.009±0.002
RuO_2-5%Sn	0.851	0.864	0.013±0.002

Table S3. Summary of structural and surface electronic properties: XRD parameters (2θ position and FWHM of the RuO_2 (110) plane, crystallite size) and XPS binding energy of Ru $3p_{3/2}$ for the RuO_2 and doped electrodes.

	XRD (RuO_2 110)			XPS (Ru $3p_{3/2}$)
	2θ (°)	FWHM (°)	D (nm)	Binding Energy (eV)
RuO_2	27.9	0.55	14.8	462.74
RuO_2-5%Mo	27.8	0.55	14.6	462.53
RuO_2-5%Ta	27.9	0.55	14.6	462.44
RuO_2-5%Zr	27.8	0.51	15.9	462.15
RuO_2-5%W	27.9	0.57	14.2	462.79
RuO_2-5%Sn	27.9	0.53	15.2	462.49

Table S4. Electrochemical performance parameters of the RuO_2 and doped electrodes.

	Onset Potential for OER (V vs. RHE)	Potential at 10 mA cm^{-2} (V vs. RHE)	Tafel Slope (mV dec^{-1})	C_{dl} (mF cm^{-2})	ECSA (cm^2 geo)
RuO_2	1.41	1.59	94.4	1.88	47
RuO_2-5%Mo	1.4	1.53	72.6	4.53	113.3
RuO_2-5%Ta	1.41	1.55	84.1	6.13	153.3
RuO_2-5%Zr	1.41	1.54	68.3	4.04	101
RuO_2-5%W	1.41	1.56	91.5	3.64	91
RuO_2-5%Sn	1.41	1.54	78.4	4.8	120

Table S5. Instantaneous current densities of the RuO_2 and doped electrodes at different times during potentiostatic electrolysis.

	10 min (mA cm^{-2})	30 min (mA cm^{-2})	60 min (mA cm^{-2})
RuO_2	21.3	23.8	23.8
RuO_2-5%Mo	30	30.1	30
RuO_2-5%Ta	57	36.4	29.6
RuO_2-5%Zr	47.4	39.7	24.8
RuO_2-5%W	32.5	34.7	34.8
RuO_2-5%Sn	39.7	37.1	34.8

Table S6. Charge transfer resistance (R_{ct}) of the RuO_2 and doped electrodes before and after electrolysis.

	fresh (Ω)	after 60 min electrolysis (Ω)
RuO_2	11.5	623.5
RuO_2-5%Mo	8.9	147
RuO_2-5%Ta	7.9	305.2
RuO_2-5%Zr	7.9	605.1
RuO_2-5%W	7.3	381
RuO_2-5%Sn	11.5	240

Table S7. Assessment of Ru dissolution after electrolysis.

	Concentration (mg/L)
RuO_2	1.0
RuO_2-5%Mo	1.5
RuO_2-10%Mo	3.7